AJNR

Intracranial aneurysms: flow analysis of their origin and progression.

C F Gonzalez, Y I Cho, H V Ortega and J Moret

AJNR Am J Neuroradiol 1992, 13 (1) 181-188
http://www.ajnr.org/content/13/1/181

Intracranial Aneurysms: Flow Analysis of Their Origin and Progression

Carlos F. Gonzalez,[1] Young I. Cho,[2] Hector V. Ortega,[1] and Jacques Moret[3]

Purpose: To explain the origin and growth of intracranial aneurysms using the hemodynamic data obtained from a computer simulation. **Materials and Methods:** Pulsatile flow in an intracranial aneurysm cavity was numerically simulated based on physiologic pulsatile flow observed in the aorta. A finite element method was applied to solve the equations of motion and the non-Newtonian viscosity of blood was taken into account in the analysis. An angiogram of a middle cerebral artery segment with aneurysm was used for the computer modeling of blood flow within the aneurysm cavity. Local shear stress and pressure on the wall at the neck of the aneurysm as well as blood flow motions inside the cavity were calculated as a function of time for various stages in the development of the aneurysm. **Findings:** Blood moves into the aneurysm cavity along the proximal wall of the cavity and emerges along the distal wall during the acceleration period of systole; however, during the deceleration period of systole and diastole, blood changes its flow direction, entering along the distal wall of the cavity and leaving along the proximal cavity wall. Rapid changes of blood flow direction result in rapid changes in wall shear stress and pressure at the proximal and distal walls of the cavity, rendering continuous damage to the intima at the cavity neck. These hemodynamic stresses relate to the anatomy of a particular vessel may be responsible for the initiation of aneurysm formation and subsequent progression, thrombosis and/or rupture. **Conclusion:** Computer modeling can further our understanding of factors that determine the origin and progression of intracranial aneurysms.

Index terms: Aneurysm, intracranial; Models, computer; Blood, flow dynamics

AJNR 13:181–188, January/February 1992

The congenital theory of the etiology of intracranial aneurysms has been widely accepted for many years, although evidence of congenital development or inherited weakness of the vessel wall is difficult to obtain (1). Hypertension and connective tissue disorders associated with acquired loss of tensile strength of the connective tissues have also been identified as possible causative factors. Recently, Stehbens pointed out that these aneurysms are acquired, degenerative lesions brought about as a result of augmented hemodynamic stress (1).

Received July 10, 1990; revision requested November 11, 1990; revision received January 2, 1991; final acceptance January 23, 1991.

[1] Department of Radiology, Thomas Jefferson University Hospital, 111 South 11th Street, Philadelphia, PA 19107. Address reprint requests to C. F. Gonzalez.

[2] Department of Mechanical Engineering, Drexel University, Philadelphia, PA 19104.

[3] Department of Interventional Neuroradiology, Fondation Adolphe de Rothschild, 29 Rue Manin, 75940 Paris, Cedex 19, France.

AJNR 13:181–188, Jan/Feb 1992 0195-6108/92/1301-0181

The hemodynamics of flow in and around aneurysms has been investigated by several researchers (2–14). In general, the intraaneurysmal flow pattern is primarily governed by the geometrical relations between the aneurysm and parent vessel. Steiger and Reulen (9) observed flow instabilities at a Reynolds number of 300 during deceleration of flow in the glass model of a cerebral saccular aneurysm and concluded that the fluctuations of flow might induce vibrations of the aneurysm wall and contribute to aneurysm progression and eventual rupture. Liepsch et al (10) conducted in vitro flow experiments and reported that the inflow into the aneurysm arose from the downstream lip and was directed toward the center of the fundus, while the backflow to the parent vessel took place along the walls of the fundus. Steiger et al (11, 12), in a similar study, reported that the size of the aneurysm had no influence on the basic pattern of intraaneurysm circulation.

It is of importance for treatment to understand the hemodynamic factors that play a role in the

formation and development of cerebral aneurysms, which include local velocity vectors, wall shear stress, and pressure. Unfortunately, previous studies which provided such information utilized experimental prototypes and measurement devices that may have disturbed physiologic functions. Alternatives to these experimental models are numerical simulation techniques. Although not a complete replacement, computer modeling (based on information easily obtained from imaging modalities such as angiography) can provide significant information about aneurysm hemodynamics.

In the present study, pulsatile flow in an intracranial aneurysm was numerically simulated. The simulation was based on physiologic pulsatile flow observed in the aorta. A finite element technique was used. This technique is a well established and highly efficient tool to solve complex problems in fluid dynamics (13). The purpose of this paper is to calculate the instantaneous flow field and wall shear stress distribution within the intraaneurysm cavity so that one can relate these hemodynamic findings to the origin and progression of intracranial aneurysms.

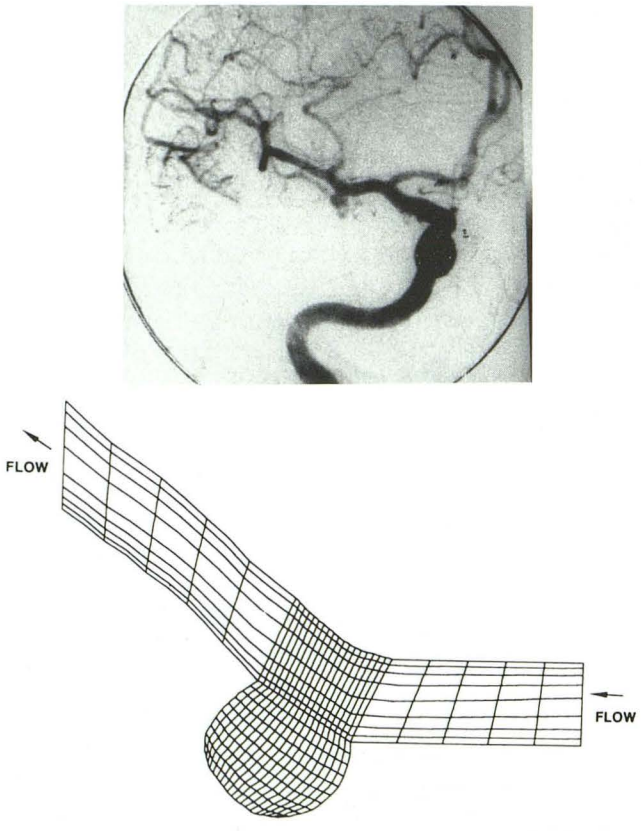

Fig. 1. Angiogram of an intracranial aneurysm of the patient and the finite element mesh for numerical computation.

Material and Methods

The angiographic appearance of a cerebral aneurysm originating in the middle cerebral artery of a patient was used for the computer modeling in this study, as shown in Figure 1. The inlet vessel diameter was 0.35 cm and the Reynolds number based on the inlet flow condition was 100. Of note is that the model studied was a two-dimensional vessel, which is an approximation of real three-dimensional flow. Thus, the circumferential motion of blood near the aneurysm could not be simulated. However, such flow is believed to be secondary to the global flow in and around the aneurysm. Also note that the flow dynamics of the three basic geometrical types of saccular aneurysm (ie, lateral, bifurcation, and terminal) are quite different. The current aneurysm can be classified as a lateral aneurysm with slight curvature, developing along the outer wall of the curved vessel. The aneurysm was chosen because of its simple anatomical configuration and because it was successfully treated by balloon occlusion. The detailed study of the hemodynamic changes produced by the introduction of a balloon within the lumen of this aneurysm is the object of a future publication.

To simulate pulsatile flow in the aneurysm, physiologic pulsatile flow observed in the aorta was chosen as the model and is shown in Figure 2, which shows a cardiac cycle of 75 beats per minute. The numerical values of the pulsatile flow are given in Appendix A in the form of relative velocity versus time. A finite element technique was used to solve the equations of the conservation of mass and momentum to obtain the velocity, pressure and wall shear stress distributions in the anatomical models. These two equations are given as

$$u_{j,j} = 0 \qquad \text{(A)}$$

$$\rho\left[\frac{\partial u_i}{\partial t} + u_j u_{j,i}\right] = -p_{,i} + \tau_{ij,j} \qquad \text{(B)}$$

where u_j is the jth component velocity vector, ρ is the density of fluid, p is the pressure, and τ_{ij} is the shear stress tensor defined by the product of the apparent viscosity (η) and the rate of strain tensor $\dot{\gamma}_{ij}$. The Galerkin formulation (15) is applied in placing the continuity and momentum equations into discrete categories. Note that the pressure term from the momentum equation is removed using the penalty formulation. Thus, a matrix equation, representing a discrete analogue of the original equations for an individual fluid element (four or nine node quadrilateral elements are used), is constructed and solved using a standard solution procedure such as the successive iteration method. The generic finite-element computer code FIDAP (15) is used to formulate and solve this matrix equation.

Although blood clearly demonstrates a shear-rate-dependent non-Newtonian viscosity (16–22), the effects of the non-Newtonian viscosity of blood on the hemodynamics of aneurysm flows are not well understood. In the present study, the non-Newtonian viscosity of the blood was taken into account by calculating the blood viscosity

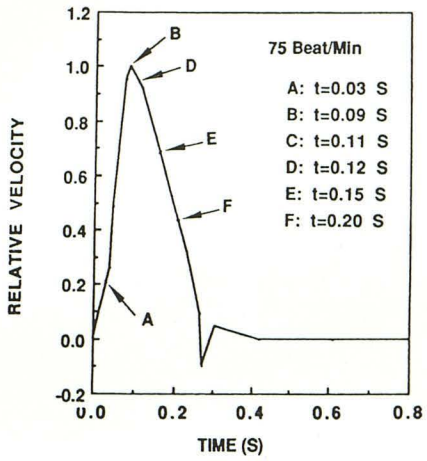

Fig. 2. Relative velocity during a cardiac cycle, defined as the instantaneous velocity divided by the maximum velocity occurring at the peak of systole. Letters *A* to *F* indicate the times as shown in the legend.

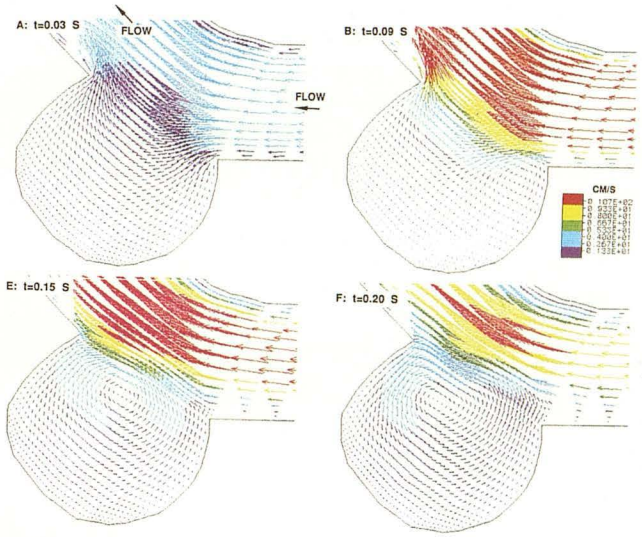

Fig. 3. Instantaneous velocity vector plots at four different times during systole: the first two (*A* and *B*) during the acceleration period and the last two (*E* and *F*) during the deceleration period. The velocity direction in the main lumen is from right to left.

locally through the second invariant of the rate of strain tensor $\dot{\gamma}_{ij}$. The detail procedure has been reported elsewhere (23) and will not be repeated here.

Results

Instantaneous velocity vectors in the aneurysm cavity are shown in Figure 3 at four different moments (A: t = 0.03 sec, B: t = 0.09 sec, E: t = 0.15 sec, and F: t = 0.20 sec). The magnitude of the velocity is indicated by the length of each line as well as by different colors. For example, flow velocities are color-coded from highest to lowest in the following order: red, yellow, green, and blue. The numerical values are given in the figure: red (10.7 cm/sec), yellow (8 cm/sec), etc. The directions of the arrows of velocity vectors represent flow direction. The first two figures (3A and 3B) represent blood flow motions during the acceleration period of systole, while the next two figures (3E and 3F) illustrate the deceleration period.

From the beginning of the systolic acceleration (A: t = 0.03 sec) to the peak of the systole (B: t = 0.095 sec), the blood enters into the aneurysm from the proximal neck side and leaves the aneurysm along the distal wall of the aneurysm as appreciated by the directions of the arrows. At the peak of systole, there is a small counterclockwise vortex near the proximal wall of the aneurysm. This small counterclockwise vortex grows as soon as deceleration starts at t = 0.12 seconds and completely dominates the aneurysm flow at t = 0.15 seconds as deceleration continues. From this moment, the counterclockwise vortex flow is continuously observed inside the aneurysm as is seen by the directions of the velocity vector arrows. In other words, blood enters the aneurysm along the distal neck and leaves the aneurysm along the proximal neck during most of the systolic deceleration process.

The hemodynamics near the distal neck is very complex. Throughout systolic acceleration blood impinges on the distal neck from the cavity side (Fig. 3, see red and blue arrows), while during the deceleration, the impingement is from the vessel side (Fig. 3, see blue arrows). In general, the blood flow in the aneurysm changes its direction during a cardiac cycle, rotating clockwise during the acceleration period and counterclockwise during most of the deceleration period. This can qualitatively be interpreted as flow fluctuations or flow instabilities. The changes in the flow direction result in directional changes in local wall shear stresses that may injure the intima, particularly at the distal neck of the aneurysm.

Figure 4 shows streamline contour plots that clearly demonstrate the local flow characteristics inside the aneurysm during cardiac systole. At the peak of systole (see B: t = 0.09 sec) a flow separation at the proximal neck and a small local recirculation near the proximal wall of the aneurysm are shown by two small curved arrows. As deceleration starts (ie, t > 0.09 sec) the small vortex near the proximal neck grows, occupying half of the aneurysm opening at t = 0.11 seconds and controlling the aneurysm flow completely at t = 0.15 seconds, as is shown by counterclockwise vortex in the aneurysm.

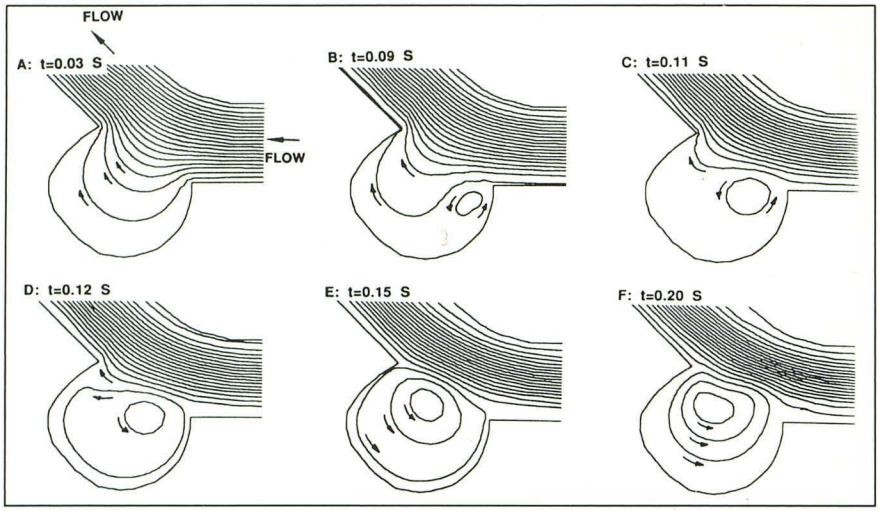

Fig. 4. Streamline contour plots at six different times (*A*, *B*, *C*, *D*, *E*, and *F*) during systole. *Arrows* are used to indicate the flow directions inside the aneurysm.

The instantaneous wall shear stress at the proximal and distal necks of the aneurysm are shown in Figure 5. The instantaneous wall shear stress varies little at the proximal neck but changes from the maximum value of 40.4 dyne/cm^2 (= 4.04 Pascal) at t = 0.08 seconds (ie, at the peak of systole) to the minimum value of −12.7 dyne/cm^2 at t = 0.20 seconds (ie, at the middle of deceleration period of systole).

In the next simulation, the size of the opening of the aneurysm is reduced and the corresponding velocity field is calculated. Figures 6 and 7 show the velocity vector plots and streamline contour plots, respectively, at four different times (A: t = 0.03 sec, B: t = 0.09 sec, E: t = 0.15 sec, and F: t = 0.20 sec). During the acceleration period of systole, the blood does not enter the aneurysm along the proximal neck, in contrast to what was observed with the broad neck aneurysm. Furthermore, the inflow along the distal neck is significantly decreased compared with the previous aneurysm. However, approaching the end of the systole (at t = 0.20 sec) there is a small inflow along the distal neck, producing a counterclockwise vortex in the aneurysm and similar to what was observed in the broad neck aneurysm but with a much reduced strength.

The instantaneous wall shear stress at the proximal and distal necks of the aneurysm with reduced opening are shown in Figure 8. The ordinate scale is chosen to be the same as one used in Figure 5 so that one can compare the effect of the aneurysm opening on wall shear stress distributions at the proximal and distal necks of the aneurysm. The instantaneous wall shear stresses both at the proximal and distal necks vary little. This demonstrates the significant effect of neck size on the hemodynamics in the aneurysm.

In an attempt to understand the etiology of this particular aneurysm, a third simulation analysis was performed on the same cerebral arterial segment but without the aneurysm. This was done by speculating the original arterial wall countour prior to development of the aneurysm; the corresponding mesh is shown in Figure 9. In the acceleration portion of systole, blood flows normally from proximal (*PR*) to distal (*DI*), as seen in the streamline countour plots at t = 0.09 seconds. During the deceleration portion of systole, the blood flow separates from the outer wall of the curved vessel segment as is seen at t = 0.15 seconds. Subsequently, this flow separation leads to a recirculation of blood flow in the area corresponding to the origin of the aneurysm, as is shown at t = 0.20 seconds. It is of note that

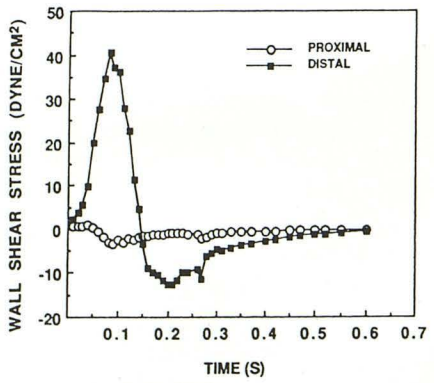

Fig. 5. Instantaneous wall shear stress calculated at the proximal (*open circles*) and distal (*closed squares*) regions of the neck of the aneurysm. Note that the magnitude and direction of the wall shear stress at the distal neck are much greater than those at the proximal neck.

the distal neck is the point where the blood flow reattaches during the deceleration period of systole.

Figure 10 shows the instantaneous wall shear stresses at the locations of proximal and distal locations. At the distal location, where the blood flow reattaches during the deceleration period of systole, the wall shear stress significantly varies from the peak value of 29 dyne/cm^2 to the minimum of −1.0 dyne/cm^2. At the proximal location, the wall shear stress changes from the

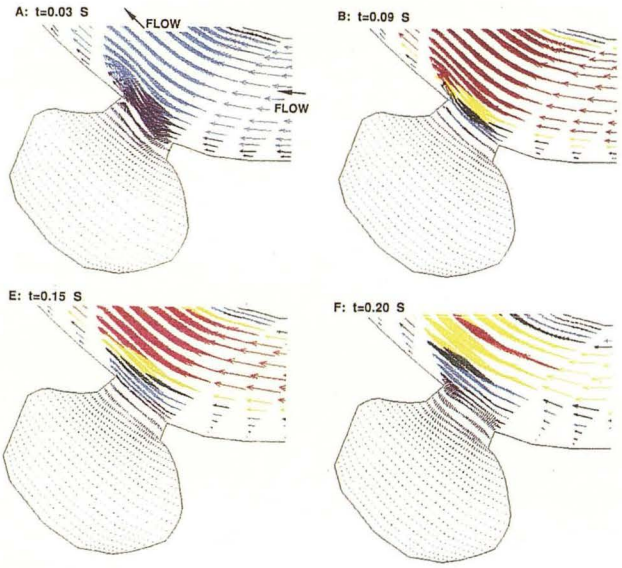

Fig. 6. Instantaneous velocity vector plots at four different times during systole in an aneurysm with reduced opening, the first two (*A* and *B*) during the acceleration period and the last two (*E* and *F*) during the deceleration period. The velocity direction in the main lumen is from right to left.

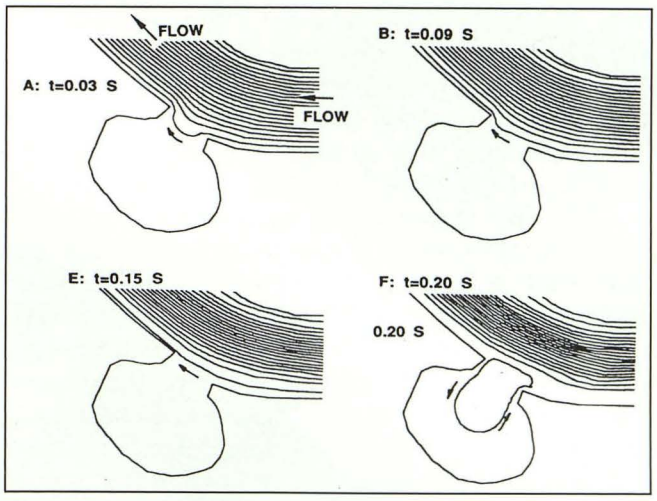

Fig. 7. Streamline contour plots at four different times (*A*, *B*, *E*, and *F*) during systole in an aneurysm with reduced opening. *Arrows* are used to indicate the flow directions inside the aneurysm.

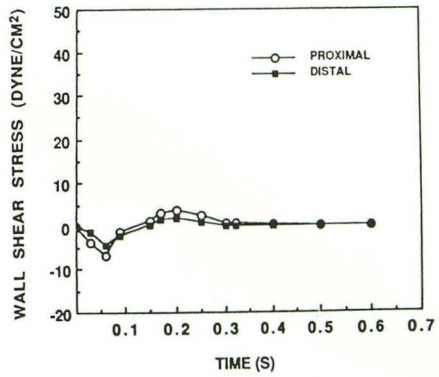

Fig. 8. Instantaneous wall shear stress calculated at the proximal (*open circles*) and distal (*closed squares*) regions of the neck of the aneurysm.

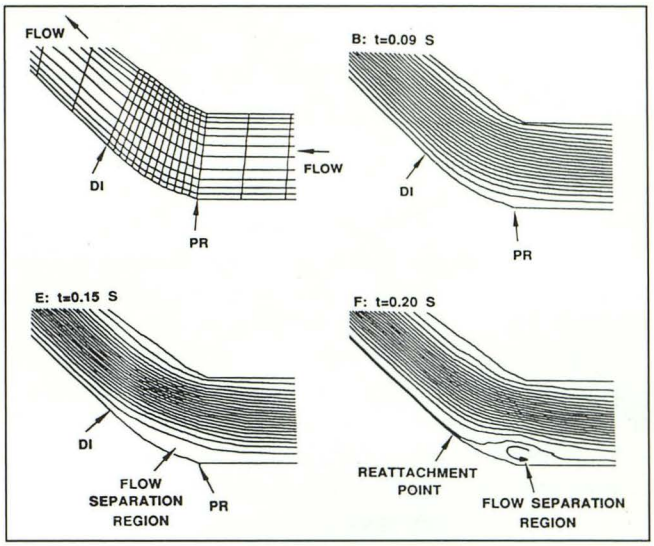

Fig. 9. Streamline contour plots at three different times (*B*, *E*, and *F*) during systole in a developing aneurysm, *PR* and *DI* indicate the locations of the proximal and distal neck regions in the aneurysm. Flow separation regions and the location of the flow reattachment point are indicated by *arrows*. The velocity direction in the main lumen is from right to left.

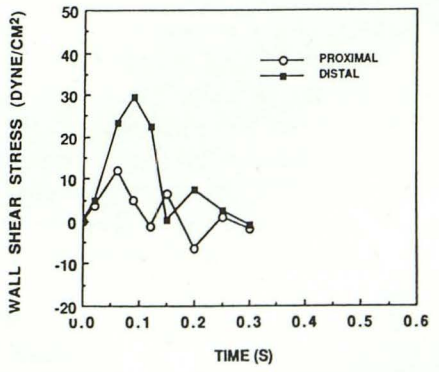

Fig. 10. Instantaneous wall shear stress calculated at proximal (*open circles*) and distal (*closed squares*) regions of developing aneurysm.

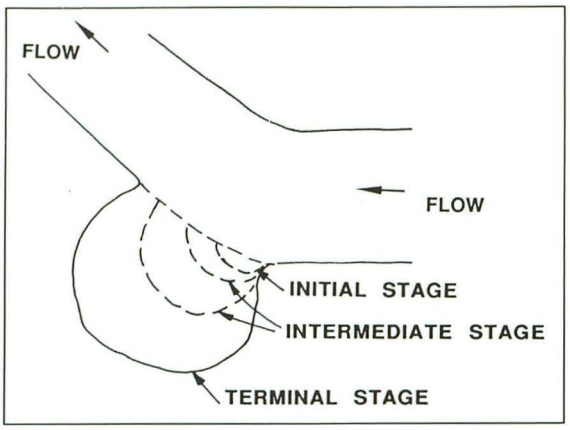

Fig. 11. A qualitative sketch of the progression of an aneurysm. The aneurysm grows from the proximal side into the distal side.

maximal value of 11.9 dyne/cm^2 to the minimum of −6.4 dyne/cm^2.

Discussion

Surgical endovascular treatment of intracerebral aneurysms has advanced significantly in the last few years. This has lead to a greater need of detailed knowledge of hemodynamic changes present in a saccular cerebral aneurysm. Information provided by hemodynamic parameters, for example, flow velocity, flow direction, and wall shear stress may aid in the selection of therapeutic approach. With the aid of our computer simulation system, we have demonstrated a number of suspected, but unproven, hypotheses that we believe play a significant role in the origin and progression of intracranial saccular aneurysms.

As suspected, the vortex flow seen within the cavity of the aneurysm is laminar (14–27). A major change in the direction of blood flow is seen during the acceleration and deceleration periods of systole (ie, clockwise rotation during the acceleration period and counterclockwise rotation during the deceleration period of systole). Such rapid changes of the impinging direction at the distal neck of the cavity that occur once in every cardiac cycle should produce a significant hemodynamic stress there. In other words, the rapid change in flow direction produces increased wall shear stress, with the probability of continuous injury to the endothelial wall (14, 29). Furthermore, we believe that the endothelial cells may not respond quickly enough to the oscillatory wall shear stress, resulting in dilation of the neck first, followed by the enlargement of the whole aneurysm. The change in the direction of the wall shear stress may be more important than the change in magnitude of wall shear stress because the intima may be much more susceptible to an oscillatory shear stress than to an unidirectional shear stress. Depending upon the weakness of the layers in the aneurysmal dome and the systemic blood pressure, the aneurysm may rupture or continue to grow, thus becoming a large or giant aneurysm.

A strong flow recirculation near the proximal portion of the neck demonstrated in Figures 3 and 4 produces oscillation of wall shear stress, possibly leading to intima injury at this site. We believe that this directional recirculation and subsequent oscillation of wall shear stress are the etiology of this lateral aneurysm. Furthermore, due to these flow disturbances, the wall shear stress particularly proximally changes its direction, which results in auxiliary shear stress that may cause continual damage to the endothelial cells. When a small aneurysm develops at the proximal location, the distal neck is a primary target of these stress effects because the blood impinges on the wall throughout the cardiac cycle. A qualitative sketch in Figure 11 shows the initial aneurysm near the proximal location and the distal neck being gradually pushed in the downstream direction, reaching the terminal position. In summary, the major changes in the hemodynamics occur at the neck and not in the dome of aneurysms as previously suspected.

Similar observations have been made by investigators studying the behavior of blood flow in glass models of aneurysms utilizing dye injections or noninvasive laser-Doppler techniques (10, 11). In experiments performed on terminal, as well as laterally located aneurysms, maximum shear stress was not found at the aneurysmal dome, but near the aneurysmal neck, which is most likely the growth matrix of the aneurysm (30–32). This concept is of particular importance if surgery or endovascular procedures such as detachable balloon obliteration or coil deposition within the cavity of an aneurysm are considered. It is quite clear that obliteration of the endothelial layers of the aneurysm neck, where the shear stress pressures are the highest, is of great importance, whether it be by surgical clipping or endovascular obliteration. If the neck of the aneurysm is not totally obliterated, rupture or recurrence of the aneurysm may result. Other critical factors in the success or failure of treatment is the size and configuration of the aneurysm neck.

Appendix A

Numerical values of the pulsatile flow in the form of a relative velocity vs time.

Time (sec)	Relative velocity
0	0
0.0381	0.262
0.0457	0.485
0.0762	0.951
0.0876	1.00
0.1143	0.922
0.1524	0.738
0.1905	0.524
0.2286	0.32
0.2667	0.0971
0.2743	−0.0971
0.3048	0.0485
0.419	0.0
0.6	0.0
0.8	0.0

A small aneurysm with a small neck probably responds better to endovascular treatment, since blood velocity within the aneurysm is diminished and a small neck is easier to obliterate. Large aneurysms with large necks are far more difficult to treat with either surgery or endovascular occlusion, since the flow patterns in large aneurysms are more complicated. This is due to blood stagnation produced by increased blood viscosity and slow flow leading to aneurysmal thrombosis (27–30). In addition, the neck is larger and therefore, more difficult to obliterate. In experimental models, flow in an aneurysm depends upon its geometric configuration and relation to the parent vessel, size of the neck and volume of the aneurysm (2–8).

Another hypothesis generated by our results relates to the causative event in the formation of an intracranial aneurysm. We believe that weakening of the arterial wall, accentuated by the previously described hemodynamic factors, and the anatomical configuration of a particular arterial vessel is responsible for the formation of saccular aneurysms. This explanation has been supported by various investigators working on experimental models and competes with the congenital theory of the origin of intracranial aneurysms, such as the media defect theory proposed by Forbus (33). According to Stebbens (34–38), there is no scientific data in support of congenital, developmental, or inherited weakness of aneurysmal walls, and the only explanation for the formation of these aneurysms is that they are acquired lesions and the result of hemodynamic stress. This hemodynamic theory may also explain why aneurysms are more prone to develop at bifurcations or trifurcations of cerebral arteries, where increased shear stress is more common. We believe, however, that biochemical or structural defects in the vessel wall facilitate production of aneurysms.

In summary, computer modeling of intracranial sacular aneurysms, based on angiographic data obtained from humans, can aid in the study and understanding of the hemodynamic factors that determine the origin and progression of intracranial aneurysms. This knowledge is important in the planning and choice of treatment of these vascular lesions.

References

1. Stehbens WE. Etiology of intracranial berry aneurysms. *J Neurosurg* 1989;70:823–831
2. Huber P. Angiographic Schichtungseffekte in den sackfoermigen Ancurysmen der Hirngefaesse. *Fortschr Roentgenstr* 1961;94:355–362
3. Huber P. Angiographische Darstellung der Zirkulationsverhaeltnisse in grossen sackfoermigen Aneurysn. *Fortschr Roentgenstr* 1966;105:773–776
4. Black SPW, German WL. Observation on the relationship between the volume and the size of the orifice of experimental aneurysms. *J Neurosurg* 1960;17:984–990
5. Ferguson GG, Roach MR. Flow conditions at bifurcations as determined in glass models, with reference to the focal distribution of vascular lesions. In: Berge VH, Derek H, eds. *Cardiovascular fluid dynamics.* London: Academic Press, 1972:141–156
6. Roach M, Scott S, Ferguson GG. The hemodynamic importance of geometry of bifurcations in the circle of Willis (glass model studies). *Stroke* 1972;3:255–267
7. Keber W, Heilman CB. Flow in experimental berry aneurysms: method and model. *AJNR* 1983;4:374–377
8. Miimi H, Kawano Y, Sugiyama I. Structure of blood flow through a curves vessel with an aneurysm. *Biorheology* 1984;21:603–615
9. Steiger HJ, Reulen HJ. Low frequency flow fluctuations in saccular aneurysms. *Acta Neurochir (Wien)* 1986;83:131–137
10. Liepsch DW, Steiger HJ, Poll A, Reulen HJ. Hemodynamic stress in lateral saccular aneurysms. *Biorheology* 1987;24:689–710
11. Steiger HJ, Poll A, Liepsch DW, Reulen HJ. Basic flow structure in saccular aneurysms: a flow visualization study. *Heart Vessels* 1987;3:55–65
12. Steiger HJ, Liepsch DW, Poll A, Reulen HJ. Hemodynamic stress in terminal saccular aneurysms: a laser-Doppler study. *Heart Vessels* 1988;4:162–169
13. Perktold K, Kenner T, Hilbert D, Spork B, Florian H. Numerical blood flow analysis: arterial bifurcation with a saccular aneurysm. *Basic Res Cardiol* 1988;83:24–31
14. Strother CM, Graves V, Partington C, Rappe A. *Hemodynamic features of human and experimental aneurysms.* Presented at 28th Annual Meeting of American Society of Neuroradiology, Los Angeles, CA, March 19–23 1990

15. FIDAP. *User's manual.* Evanston, IL: Fluid Dynamics International, Inc., 1990
16. Wells RE, Denton R, Merrill EW. Measurement of viscosity of biologic fluids by Cone Plate Viscometer. *J Lab Clin Med* 1961;57:646–656
17. Rand PW, Lacombe E, Hunt HE, Austin WH. Viscosity of normal human blood under normothemic and hypothemic conditions. *J Appl Physiol* 1964;19:177–182
18. Schmid-Schonbein H, Wells RE Jr, Goldstone J. Fluid drop-like behavior of erythrocytes: disturbance in pathology and its quantification. *Biorheology* 1971;7:227–234
19. Evans RL, Kirkwood RB, Opsahl DG. The dynamic viscosity of some human blood. *Biorheology* 1971;8:125–128
20. Skalak R, Keller SR, Secomb TW. Mechanics of blood flow. *J Biomech Eng* 1981;103:102–115
21. Biro GP. Comparison of acute cardiovascular effects and oxygen-supply following haemodilution with dextran, stroma-free haemoglobin solution and fluorocarbon suspension. *Cardiovascular Res* 1982;16:194–204
22. Dintenfass L. *Blood viscosity, hyperviscosity and hyperviscosaemia.* Lancaster, England: MTP Press Ltd, 1985:21, 23–24, 141
23. Cho YI, Kensy KR. Effects of the non-Newtonian viscosity of blood on hemodynamics of diseased arterial flows. *1989 Advances in Bioengineering BED* 1989;15:147–148
24. Liepsch DW. Untersuchungen der stroemungsverhaeltnisse in verzweigungen von Rohren kleiner Duchmesser bei Stromtrennung. *Diss TU Munich u VDI Berichte* 1975;232:423–441
25. Liepsch DW, Moravec S. Pulsatile flow of non-Newtonian fluid in distensible models of human arteries. *J Biorheol* 1984;21:271–586
26. Liepsch DW, Moraves S, Rastogi AK, Vlachos ND. Measurement and calculations of laminar flow in a ninety degree bifurcation. *J Biomech* 1983;15:753–766
27. Liepsch DW. Flow in tubes and arteries: a comparison. *Biorheology* 1986;23:395–433
28. Fry DL. Certain histological and chemical responses of the vascular interface to acutely induced mechanical stress in the aorta of the dog. *Circ Res* 1969;14:93–108
29. Fry DL. Certain histological and chemical responses of the vascular interface to acutely induced mechanical stress in the aorta of the dog. *Circ Res* 1968;22:165–197
30. Stokes VK. Couple stresses in fluids. *The physics of fluids* 1966;9:1709–1715
31. Suzuki J, Ohara H. Clinicopathological study of cerebral aneurysms. *J Neurosurg* 1978;48:505–514
32. Tognetti F, Limoni P, Testa C. Aneurysm growth and hemodynamic stress. *Surg Neurol* 1983;20:74–78
33. Forbus WD. On the origin of miliary aneurysms of the superficial cerebral articles. *Bull Johns Hopkins Hosp* 1930;47:239:284
34. Stehbens WE. An etiology of cerebral aneurysms. *Lancet* 1981;2:524–525
35. Stehbens WE. Aneurysms and anatomical variations of cerebral arteries. *Arch Pathol* 1963;75:45–64
36. Stehbens WE. Arterial structure at branches and bifurcations with reference to physiological and pathological processes, including aneurysm formation. In: Schwartz CJ, Werthessen NT, Wolf S, eds. *Structure and function of the circulation.* New York: Plenum Press, 1981;2:667–693
37. Stehbens WE. Atypical cerebral aneurysms. *Med J Aust* 1965;1: 765–767
38. Stehbens WE. Cerebral aneurysm and congenital abnormalities. *Aust Ann Med* 1962;11:102–112